JACS
JOURNAL OF THE AMERICAN CHEMICAL SOCIETY
ARTICLE
pubs.acs.org/JACS

Large-Scale Synthesis of Uniform and Extremely Small-Sized Iron Oxide Nanoparticles for High-Resolution T_1 Magnetic Resonance Imaging Contrast Agents

Byung Hyo Kim,[†,⊥] Nohyun Lee,[†,⊥] Hyoungsu Kim,[‡] Kwangjin An,[†] Yong Il Park,[†] Yoonseok Choi,[‡] Kwangsoo Shin,[†] Youjin Lee,[†] Soon Gu Kwon,[†] Hyon Bin Na,[†] Je-Geun Park,[§] Tae-Young Ahn,[∥] Young-Woon Kim,[∥] Woo Kyung Moon,[‡] Seung Hong Choi,[*,‡] and Taeghwan Hyeon[*,†]

[†]World Class University Program of Chemical Convergence for Energy & Environment, and School of Chemical and Biological Engineering, and [∥]Department of Materials Science and Engineering, Seoul National University, Seoul 151-744, Korea

[‡]Diagnostic Radiology, Seoul National University Hospital, and the Institute of Radiation Medicine, Medical Research Center, Seoul National University, Seoul 110-744, Korea

[§]Department of Physics, Seoul National University, Seoul 151-742, Korea

Supporting Information

ABSTRACT: Uniform and extremely small-sized iron oxide nanoparticles (ESIONs) of < 4 nm were synthesized via the thermal decomposition of iron−oleate complex in the presence of oleyl alcohol. Oleyl alcohol lowered the reaction temperature by reducing iron−oleate complex, resulting in the production of small-sized nanoparticles. XRD pattern of 3 nm-sized nanoparticles revealed maghemite crystal structure. These nanoparticles exhibited very low magnetization derived from the spin-canting effect. The hydrophobic nanoparticles can be easily transformed to water-dispersible and biocompatible nanoparticles by capping with the poly(ethylene glycol)-derivatized phosphine oxide (PO-PEG) ligands. Toxic response was not observed with Fe concentration up to 100 μg/mL in MTT cell proliferation assay of POPEG-capped 3 nm-sized iron oxide nanoparticles. The 3 nm-sized nanoparticles exhibited a high r_1 relaxivity of 4.78 mM^{-1} s^{-1} and low r_2/r_1 ratio of 6.12, demonstrating that ESIONs can be efficient T_1 contrast agents. The high r_1 relaxivities of ESIONs can be attributed to the large number of surface Fe^{3+} ions with 5 unpaired valence electrons. In the in vivo T_1-weighted magnetic resonance imaging (MRI), ESIONs showed longer circulation time than the clinically used gadolinium complex-based contrast agent, enabling high-resolution imaging. High-resolution blood pool MR imaging using ESIONs enabled clear observation of various blood vessels with sizes down to 0.2 mm. These results demonstrate the potential of ESIONs as T_1 MRI contrast agents in clinical settings.

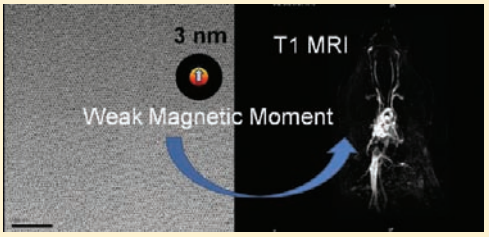

INTRODUCTION

Magnetic resonance imaging (MRI) is one of the most powerful medical diagnosis tools because MRI can provide images with excellent anatomical details based on the soft tissue contrast and functional information in noninvasive and real-time monitoring manner.[1,2] The sensitivity of MRI can be greatly improved by the contrast agents that enhance the contrast of the region of interest from background. The MRI contrast agents are generally categorized according to their effects on longitudinal (T_1) and transversal (T_2) relaxations, and their ability is referred to as relaxivity (r_1, r_2). The area wherein fast T_1 relaxation takes place appears bright, whereas T_2 relaxation results in the dark contrast in the MR images.

Superparamagnetic iron oxide nanoparticles (SPIO) such as Feridex are the representative T_2 contrast agents.[2] Magnetic nanoparticles provide T_2 contrast effect due to the magnetic inhomogeneity induced by their strong magnetic moment.[2f] Wide clinical uses of the magnetic nanoparticle-based T_2 contrast agents were hampered by several disadvantages.[1a] First, the intrinsic dark signal in T_2-weighted MRI can mislead the clinical diagnosis because lesions and tumors labeled with T_2 agents can be confused with other hyphointense areas such as bleeding, calcification, or metal deposition. Moreover, the high magnetic moment of T_2 contrast agents induces the perturbation of local magnetic field, causing the so-called "blooming effect". This effect exaggerates the size of labeled area and blurs the image.[3] For these reasons, T_1 contrast agent is more desirable than T_2 agent for the accurate high-resolution imaging.[1b]

Paramagnetic compounds with large number of unpaired electrons including Gd^{3+}, Mn^{2+}, and Fe^{3+} are desirable for T_1 contrast agents because T_1 contrast effect is induced by the interactions between protons of water molecules and electron spins of the contrast agents. Gadolinium complexes such as Gd-DOTA, having 7 unpaired electrons in its Gd^{3+} core, are widely used as T_1 contrast agent.[4] However, the gadolinium complexes

Received: April 12, 2011
Published: July 11, 2011

have several disadvantages in clinical settings. The complexes generally have short circulating time due to rapid excretion through urine, which hampers the high-resolution imaging that requires long scan time. In addition, they cannot be easily functionalized with various functional materials. Most importantly, free gadolinium ions, leached from gadolinium complexes, are known to be very toxic. For example, recently FDA warned on association regarding gadolinium-based MR contrast agents and nephrogenic system fibrosis (NSF), which is a very serious syndrome and is known to be caused by free released gadolinium ions.[5a]

To overcome these disadvantages of Gd-complex based T_1 MRI contrast agents, development of nanoparticulate T_1 contrast agents that containing Gd^{3+} or Mn^{2+} ions has been intensively pursued in recent years.[6−8] However, toxicity problem still persists in these nanoparticle-based T_1 contrast agents.[5] Consequently, further optimization of the contrast agents is required for ultrasensitive imaging and early diagnosis of diseases. In particular, new nontoxic T_1 MRI contrast agents should be developed to overcome the drawbacks of not only the negative contrast effect of T_2 agents but also the toxicity of Gd-based T_1 agents.

Iron oxide is more biocompatible than gadolinium- or manganese-based materials because the iron species are rich in human blood, which are mostly stored as ferritin in the body. However, common iron oxide nanoparticles are not appropriate for the T_1 MRI contrast agents because the ideal T_1 contrast agents should have high r_1 value and low r_2/r_1 ratio to maximize the T_1 contrast effect. Although ferric (Fe^{3+}) ions having 5 unpaired electrons increase the r_1 value, the high r_2 of iron oxide nanoparticles derived from innate high magnetic moment prevents them from being utilized as T_1 contrast agent. This problem can be resolved by decreasing size of the magnetic nanoparticles.[9] The magnetic moment of magnetic nanoparticles rapidly decreases as their sizes decrease due to the reduction in the volume magnetic anisotropy and spin disorders on the surface of the nanoparticles.[10] The small size iron oxide nanoparticles are the potential candidate for T_1 contrast agents because the nanoparticles can enhance the T_1 effect by their large surface area with 5 unpaired electrons, suppress the T_2 effect by their small magnetic moment, and have low toxicity. Moreover, the nanoparticles are advantageous for funtionalization and long-term imaging. It has been shown that small-sized iron oxide nanoparticles such as ultrasmall particles of iron oxide (USPIO) can be utilized as T_1 contrast agents.[11] However, the nanoparticles in the previous reports were larger than 4 nm and still exhibited appreciable magnetic moment.

MR relaxivity is strongly related to the size of the nanoparticles. Therefore, size-controlled synthesis of uniform nanoparticles is critical for the fine control of MR relaxivity.[12] Uniform iron oxide nanoparticles have been synthesized by various methods including the thermal decomposition process.[13,14] However, there are very few reports on the synthesis of iron oxide nanoparticles smaller than 3 nm.[15] Moreover, these previous methods have some limitations for large-scale synthesis due to the low yield and high cost of reagents. In this Article, we report on the synthesis of uniform and extremely small-sized iron oxide nanoparticles (ESIONs) of sizes down to 1.5 nm using the heat-up method. The synthetic procedure is simple, cost-effective, and easy to scale up. Furthermore, the nanoparticles were successfully used as T_1 MRI contrast agents for the high-resolution angiography.

EXPERIMENTAL SECTION

Synthesis of Iron Oxide Nanoparticles. Iron−oleate complex was synthesized according to the previously reported procedure.[13] For the synthesis of 3 nm-sized iron oxide nanoparticles, 1.8 g of iron-oleate complex (2 mmol), 0.57 g of oleic acid (2 mmol), and 1.61 g of oleyl alcohol (6 mmol) were dissolved in 10 g of diphenyl ether at room temperature. The mixture was heated to 250 °C at a constant heating rate of 10 °C/min and then kept at this temperature for 30 min under inert atmosphere. As the reaction proceeded, the initial brown transparent solution became black. After the reaction, the mixture containing the nanoparticles was rapidly cooled to room temperature, and 50 mL of acetone was added to precipitate the nanoparticles. The nanoparticles were separated by centrifugation and dispersed in nonpolar solvent such as *n*-hexane or chloroform. To obtain 2.2 nm-sized nanoparticles, 1.8 g of iron−oleate complex (2 mmol) and 3.22 g of oleyl alcohol (12 mmol) were mixed in 10 g of diphenyl ether at room temperature and heated by the same heating procedure as that for 3 nm-sized nanoparticles.

Ligand Exchange of Iron Oxide Nanoparticles with PO-PEG. PEG-derivatized phosphine oxide (PO-PEG) was synthesized according to the previously reported method.[16] In a typical procedure, 10 mg of 3 nm-sized iron oxide nanoparticles and 200 mg of PO-PEG were mixed in 1 mL of ethanol and 1 mL of *n*-heptane.[17] Next, the mixture was heated slowly to 70 °C and kept at this temperature for 5 h. After the reaction, *n*-hexane was added to precipitate PO-PEG coated nanoparticles, which were collected by centrifugation and redispersed in ethanol. Finally, the nanoparticles were dispersed in distilled water, and the remaining ethanol was removed by evaporation.

MRI Relaxation Properties of Iron Oxide Nanoparticles. MR relaxivities of iron oxide nanoparticles were measured using a clinical 3 T MR scanner (Siemens, TrioTrim) with a head coil. IR-FSE sequence was used to measure T_1. The measurement parameters were as follows: TR = 4000 ms, TE = 14 ms, and TI = 25−3500 ms. CPMG sequence was used to measure T_2, and its parameters were TR = 5000 ms and TE = 16−200 ms.

In Vitro MR Imaging. MCF-7 cells (human breast cancer cell line) were grown in monolayer in Dulbecco's Modified Eagle's Medium (DMEM, WelGENE) supplemented with 10% (v/v) fetal bovine serum (FBS, Gibco) and penicillin/streptomycin (100 U/mL and 100 g/mL, respectively, Gibco) in a humidified 5% CO_2 atmosphere at 37 °C. To label the cells with iron oxide nanoparticles, the cells were seeded onto culture dishes in 10 mL of media and grown overnight. Subsequently, 3 and 12 nm-sized iron oxide nanoparticles of 0, 25, and 100 μg/mL were added. After 24 h, the cells were washed twice with PBS and detached by adding 1 mL of trypsin/EDTA. After centrifugation, cells were dispersed in culture media and transferred to a 1.5 mL test tube. Cell pellets were prepared by centrifugation at 1000 rpm for 5 min. T_1 weighted MR images were acquired with a head coil on a 1.5 T MR scanner (GE Signa Excite, Milwaukee, WI). The imaging parameters were as follows: flip angle = 90, ETL = 1, TR = 500 ms, TE = 11 ms, field of view FOV = 200 × 200 mm^2, matrix = 320 × 192, slice thickness/gap = 1.0 mm/2.5 mm, and NEX = 1.

In Vivo MR Imaging. Dynamic time-resolved MR angiography and 3d-FLASH images of rats were acquired using a wrist coil on a 3 T MRI scanner before and after the injection of iron oxide nanoparticles (2.5 mg Fe/kg). The precontrast images were subtracted from post-contrast images, and the resulting images were reconstructed using maximum intensity projection (MIP) protocol with OsriX (Version 3.8.1; 32bit; OsiriX foundation, Geneva). Dynamic time-resolved MR angiography was obtained with an interpolated temporal resolution of 1.25 s and the following parameters: flip angle = 20, ETL = 1, TR = 3.1 ms, TE = 1.13 ms, field of view FOV = 75 × 140 mm^2, matrix = 256 × 106, slice thickness/gap = 2.5 mm/0 mm, and NEX = 1. The imaging parameters of 3d-FLASH are as follows: flip angle = 25,

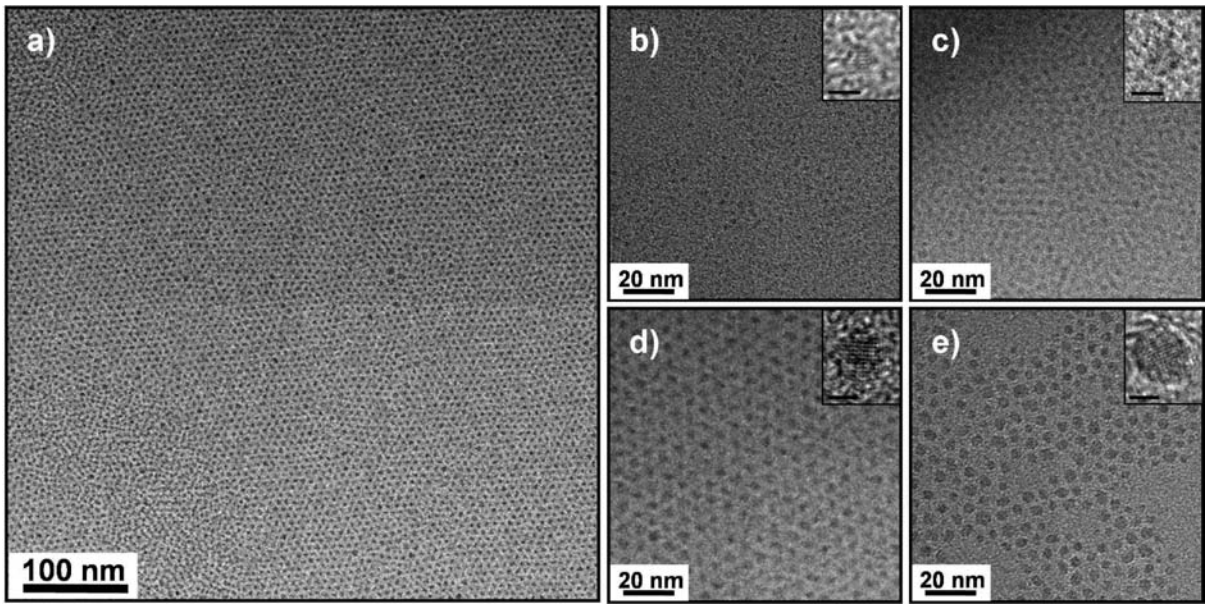

Figure 1. (a,d) TEM images of 3 nm-sized iron oxide nanoparticles at the magnifications of (a) 40k and (d) 200k. (b−e) TEM images of iron oxide nanoparticles with diameters of (b) 1.5 nm, (c) 2.2 nm, (d) 3 nm, and (e) 3.7 nm. In the inset of (b)−(e), high-resolution TEM images of a nanoparticle are shown, and the scale bar is 2 nm. The reaction conditions are summarized in Table 1.

Table 1. Reaction Conditions for the Synthesis of ESIONs

Figure	oleyl alcohol (mmol)	oleic acid (mmol)	solvent	heating rate (°C/min)	aging temperature (°C)	size (nm)
*1*a,d	6	2	diphenyl ether	10	250	3.05 ± 0.56
*1*b	12	0	diphenyl ether	10	200	1.54 ± 0.44
*1*c	12	0	diphenyl ether	10	250	2.19 ± 0.36
*1*e	6	2	1-octadecene	10	280	3.74 ± 0.56

ETL = 1, TR = 25 ms, TE = 5.1 ms, field of view FOV = 110 × 65 mm^2, matrix = 256 × 169, slice thickness/gap = 1.0 mm/0 mm, and NEX = 2.

RESULTS AND DISCUSSION

Synthesis of Iron Oxide Nanoparticles. Extremely small iron oxide nanoparticles (ESIONs) with their size < 4 nm were synthesized by thermal decomposition of iron−oleate complex in the presence of oleic acid and oleyl alcohol in diphenyl ether. Figure 1a shows that 3 nm-sized ESIONs are assembled into ordered array on TEM grid due to their excellent size uniformity. The high-resolution TEM image in the inset of Figure 1d clearly shows crystal lattice of the nanoparticles, demonstrating their high crystallinity. Their size could be finely controlled from 1.5 to 3.7 nm, as shown in Figure 1b−e. Detailed reaction conditions are summarized in Table 1. The size of the nanoparticles could be decreased by increasing the ratio of oleyl alcohol to oleic acid. When the reaction mixture composed of 2 mmol of iron−oleate complex, 6 mmol of oleyl alcohol, 2 mmol of oleic acid, and 10 g of diphenyl ether was aged at 250 °C, uniform 3 nm-sized ESIONs were produced (Figure 1d). In the absence of oleic acid, 2.2 nm-sized ESIONs were obtained (Figure 1c). The size of ESIONs could also be controlled by changing the aging temperature. When the reaction mixture for the synthesis of 2.2 nm-sized nanoparticles was aged at 200 °C, 1.5 nm-sized ESIONs could be synthesized (Figure 1b). When the reaction mixture composed of 2 mmol of iron−oleate complex, 6 mmol of oleyl alcohol, 2 mmol of oleic acid, and 10 g of 1-octadecene were aged at 280 °C, 3.7 nm-sized nanoparticles were obtained (Figure 1e).

XRD pattern of 3 nm-sized nanoparticles revealed maghemite (γ-Fe_2O_3; JCPDS no. 39-1346) crystal structure (Figure S1 in the Supporting Information). Although a clear distinction between magnetite and maghemite is difficult because XRD patterns of these two crystal structures are very similar, the XRD pattern matched well with maghemite (Table S1 in the Supporting Information). The previous structural characterizations of 4 nm-sized iron oxide nanoparticles using X-ray absorption spectroscopy (XAS) and X-ray magnetic circular dichroism spectroscopy (XMCD) showed that the nanoparticles are predominantly maghemite.[13,14j] When the XRD pattern was compared to that of 12 nm-sized nanoparticles, the peaks of the 3 nm-sized nanoparticles were shifted to higher angles and were broader.[18] The particle size of the nanoparticles calculated by Debye−Scherrer equation from (311) peak was 3.0 nm, which matched very well with that obtained from the TEM image. ESIONs were highly stable in nonpolar solvents such as chloroform for several months without any precipitation. The current synthetic method can be easily scaled up. For example, 5 g of 3 nm-sized ESIONs could be prepared from a single batch reaction using 40 mmol of iron−oleate complex in a 1 L reactor (Figure S2 in the Supporting Information).

Although the exact formation mechanism is not clear, there is evidence that the presence of oleyl alcohol plays a critical role in

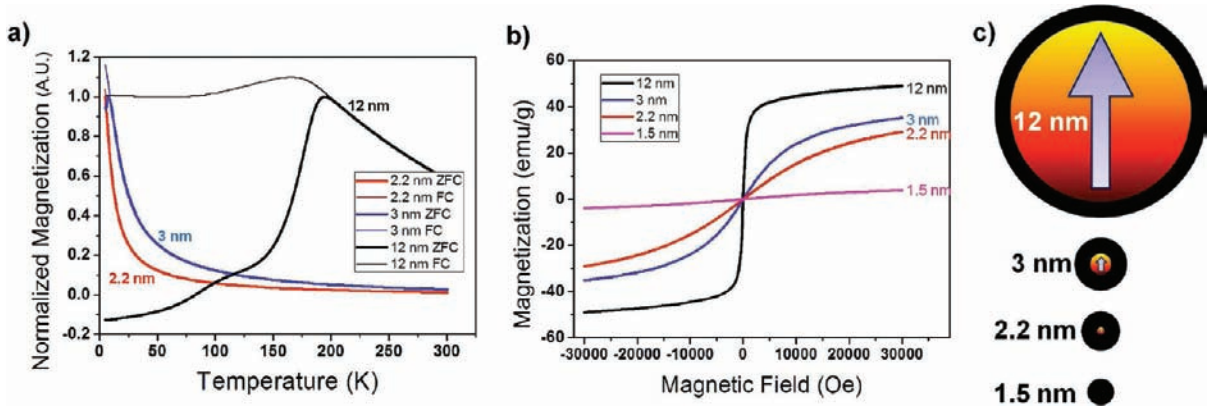

Figure 2. (a) Temperature-dependent magnetization curves ($M-T$) for iron oxide nanoparticles with diameters of 2.2 nm (red), 3 nm (blue), and 12 nm (black) measured after zero-field cooling (ZFC) and field cooling (FC) at the applied field of 100 Oe. The magnetization data were normalized with the value at the maximum of zero-field cooling magnetization. (b) Field-dependent magnetization curves ($M-H$) at 300 K for iron oxide nanoparticles with diameters of 1.5 nm (pink), 2.2 nm (red), 3 nm (blue), and 12 nm (black). (c) Description of the spin canting effect (canting layer = 0.9 nm) in the various sized iron oxide nanoparticles. Red and black colors represent magnetic cores and magnetically disordered shells.

the synthesis of the nanoparticles smaller than 3 nm. FT-IR spectra of the sample aliquots drawn from the reaction mixture during the heating procedure clearly showed that oleyl alcohol was oxidized to aldehyde during the reaction (Figure S3 in the Supporting Information), indicating that oleyl alcohol acts as a mild reductant. Reduced iron atoms seem to be released from the iron−oleate complex and can lead to subsequent nucleation and growth of the nanoparticles.[14a,b,19] No particle was formed in the absence of oleyl alcohol while keeping all of the other reaction conditions unchanged (Figure S4a in the Supporting Information). When other mild reductants such as oleylamine or 1,2-hexadecanediol were used in the synthesis, the small-sized nanoparticles could also be obtained at the aging temperature of 250 °C, but they were not as uniform as those synthesized using oleyl alcohol (Figure S4b,c in the Supporting Information). The role of oleyl alcohol in the synthesis of ESIONs can be explained as follows. In the previous heat-up process for the synthesis of iron oxide nanoparticles, thermal decomposition of iron−oleate complex, which commenced at ~300 °C, led to the formation of nanoparticles.[13,20] When the aging temperature was decreased to < 250 °C, the thermal decomposition reaction was too slow to control nucleation and growth processes, consequently resulting in polydisperse nanoparticles.[13] On the other hand, when oleyl alcohol was used as the reductant, an additional reaction pathway was provided for the release of iron atoms from the iron−oleate complex at much lower temperature. The lowered reaction temperature has a positive effect on the synthesis of the smaller nanoparticles. During the nucleation process for the synthesis of colloidal nanoparticles, a significant portion of generated nuclei dissolves back into the solution because the supersaturation level is lowered by the nucleation.[20,21] When the reaction temperature is lowered, the dissolution of nuclei is thermodynamically suppressed, increasing the number of nuclei in the reaction mixture. Given that the crystallization yield is the same, as more particles are generated, the particle size will decrease. To verify the assumption that smaller nanoparticles are synthesized at lower reaction temperatures, a fixed amount of oleyl alcohol was injected into the solution containing iron−oleate complex at the temperatures ≤ 280 °C, where the thermal decomposition of iron−-oleate complex is very slow. When oleyl alcohol was injected into the reaction mixture at the temperatures of 250, 260, and 280 °C, 3, 5, and 11 nm-sized nanoparticles were generated, respectively (Figure S5 in the Supporting Information). This result provides strong evidence for our hypothesis that the synthetic temperature can be lowered by introducing a reduction pathway, resulting in the formation of the nanoparticles smaller than 3 nm, which was very hard to obtain in the previous synthetic methods.

Magnetic Properties. Magnetic properties are strongly dependent on the particle size.[22] The magnetic properties of ESIONs with various sizes and 12 nm-sized iron oxide nanoparticles, for comparison purpose, were measured using a vibrating sample magnetometer (VSM) with the magnetic field up to 3 T and the temperature ranging from 5 to 300 K. From the temperature-dependent magnetization curve after zero-field-cooling (ZFC-MT), the blocking temperatures (T_B) of the 12, 3, and 2.2 nm-sized particle were measured to be 197, 8, and < 5 K, respectively (Figure 2a). Field-dependent magnetization ($M-H$) curves of the 1.5, 2.2, 3, and 12 nm-sized iron oxide particles are shown in Figure 2b and Figure S6 in the Supporting Information. In contrast to typical superparamagnetic nanoparticles, coercivity and remanence of ESIONs are negligible at 5 K for their very low volume anisotropy. Because MR images are usually obtained at room temperature, the magnetic properties at room temperature are important. As the particle size decreases, the magnetization at room temperature tends to decrease, especially for the nanoparticles smaller than 3 nm (Figure 2b). It is known that the spin canting effect, which results from the lack of full alignment of the spins in surface atoms, is known to be responsible for the low magnetization of small-sized magnetic nanoparticles.[23] The iron oxide nanoparticles can be regarded as core/shell structures composed of magnetic core and magnetically disordered shell.[24] The thickness of the spin canted surface layer of maghemite is known to be 0.5−0.9 nm.[23] When the spin canted layer is assumed as 0.9 nm,[23b] 93.6% of spins in 3 nm-sized iron oxide nanoparticles are canted, whereas only 38.6% of spins in 12 nm-sized nanoparticles are canted (Figure 2c). In the case of 2.2 nm-sized nanoparticles, only 0.6% of the spins are not canted. The dramatically decreased magnetization of ESIONs can be explained by the significant shrinkage of magnetic core. Magnetic moment per particle also dramatically decreased with decreasing particle size. The magnetic moments at room

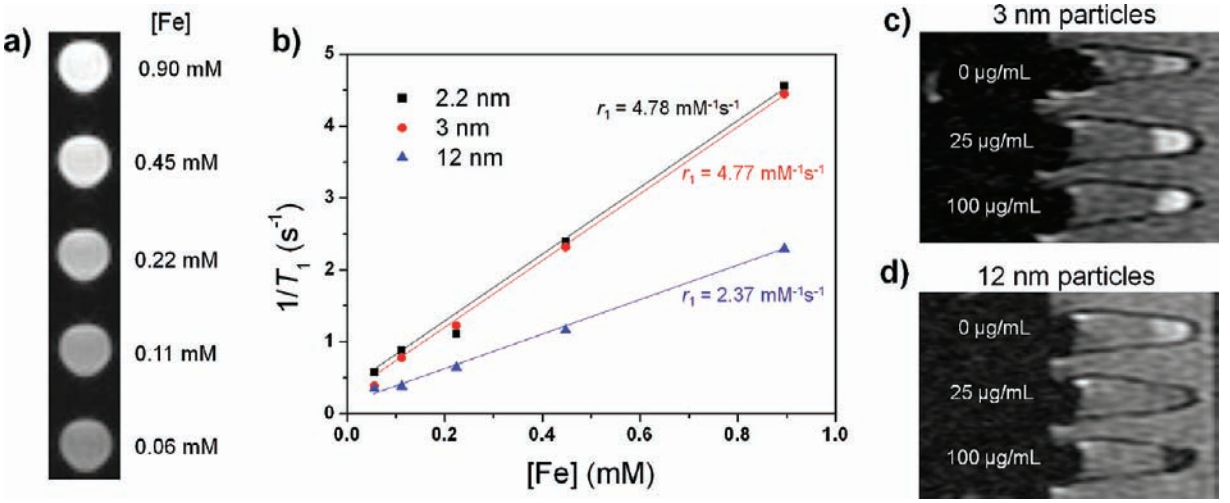

Figure 3. (a) T_1 weighted MR images of 3 nm-sized iron oxide nanoparticles. (b) Plot of $1/T_1$ over Fe concentration of iron oxide nanoparticles with diameters of 2.2 nm (■), 3 nm (red ◆), and 12 nm (blue ▲). The slope indicates the specific relaxivity (r_1). (c,d) T_1 weighted MR images of MCF-7 cell pellets after 24 h incubation with iron oxide nanoparticles with diameters of (c) 3 nm and (d) 12 nm.

temperature for 1.5, 2.2, 3, and 12 nm-sized nanoparticle were 3.91, 83.9, 273, and 24 800 μ_B, respectively, calculated by the equation, $m = M\rho V$, where M is the mass magnetization of the particle and ρ is the density of the particle.[25] The extremely low magnetic moment of ESIONs can be attributed to the small particle volume and spin canting effect.

MR Phantom Test. For various biomedical applications, it was necessary to make hydrophobic ESIONs dispersible in aqueous media. Poly(ethylene glycol)-derivatized phosphine oxide (PO-PEG) ligand was introduced via the ligand exchange reaction because of their effective reaction, biocompatibility, and low cost.[16] Coordinating phosphine-oxide headgroup strongly binds to the iron oxide core, and the poly ethyleneglycol (PEG) tail group endows the nanoparticles with colloidal stability in the aqueous media. Hydrophobic nanoparticles and PO-PEG were added into the solvent mixture composed of 1:1 of ethanol and *n*-heptane, followed by incubation at 70 °C for 5 h to promote ligand exchange reaction. The resulting PO-PEG capped 3 nm-sized ESIONs were kept stable in phosphate buffered saline (PBS) for more than 2 weeks. The hydrodynamic diameter of the particles was 15.0 nm (Figure S7 in the Supporting Information). This small overall particle size is beneficial for increasing blood half-life by avoiding uptake by the reticuloendothelial system (RES).[26] The in vitro cytotoxicity of PO-PEG capped ESIONs was evaluated by 3-[4,5-dimethylthialzol-2-yl]-2,5-diphenyltetrazolium bromide (MTT) assay. Toxic response was not observed with Fe concentration up to 100 mg/mL in MCF-7 cell (Figure S8 in the Supporting Information). The low cytotoxicity of ESIONs was also assessed by calcein-acetoxymethyl ester (AM)/propium iodide (PI) staining and 7-aminoactinomycin D (7-AAD) assays (Figures S9 and S10 in the Supporting Information).

To examine the feasibility of using ESIONs as T_1 MRI contrast agent, the relaxation time of ESIONs was measured on a 3 T clinical MR scanner. Figure 3a shows the T_1 weighted MR images of 3 nm-sized PO-PEG capped ESIONs at different concentrations. The test tubes containing higher concentration of ESIONs appeared brighter on T_1 weighted images. The r_1 relaxivities of 3 and 2.2 nm-sized ESIONs were 4.77 and 4.78 mM^{-1} s^{-1}, respectively, which were relatively high values among the reported relaxivities of the nanoparticulate T_1 contrast agents (Figure 3b).[7,11] The high r_1 relaxivities of ESIONs can be attributed to large number of Fe^{3+} ions with 5 unpaired electrons on the surface of the ESIONs. Because of the strong susceptibility effect and small surface area of 12 nm-sized iron oxide nanoparticles, their r_1 value (2.37 mM^{-1} s^{-1}) was lower than those of ESIONs. The r_2 values of 2.2, 3, and 12 nm-sized nanoparticles were 17.5, 29.2, and 58.8 mM^{-1} s^{-1}, respectively (Table 2). Because low magnetic moment induces weak magnetic inhomogeneity around the particles, ESIONs exhibit low T_2 relaxivity as compared to the larger sized particles. The r_2/r_1 ratio is an important parameter to estimate the efficiency of T_1 contrast agents. The r_2/r_1 ratios of 2.2, 3, and 12 nm-sized iron oxide nanoparticles were 3.67, 6.12, and 24.8, respectively (Table 2), demonstrating that ESIONs can be efficient T_1 contrast agents.

The uptake of 3 nm-sized ESIONs was confirmed by confocal laser scanning microscopy following the incubation of cells with the nanoparticles in serum containing cell culture media. To obtain fluorescence image, the nanoparticles were conjugated with rhodamine-B-isothiocyanate (RITC). In confocal microscopy images, the internalization of ESIONs was observed in the cytoplasm (Figure S11 in the Supporting Information). Cellular uptake of ESIONs was also assessed by an inductively coupled plasma mass spectrometer (ICP-MS), and the result was 0.17 pg of iron per cell.[27]

In vitro T_1 weighted MR images of MCF-7 cells incubated with various concentrations of the nanoparticles (0, 25, 100 μg Fe/mL) were obtained on a 1.5 T MR scanner. Significant T_1 signal enhancement was observed for the cells labeled with 25 and 100 μg Fe/mL of ESIONs, while nonlabeled cells were not brightened (Figure 3c). Although nanostructured materials are usually clustered in the endosome,[28] ESIONs provide T_1 contrast effect not only in deionized water but also in the cellular environment resulting from their low volume anisotropy. In contrast, in the cell phantom T_1 weighted MR image, the cells labeled with 12 nm-sized particles showed much less signal enhancement; even they were darkened at the high concentration (Figure 3d). The attenuated T_1 signal of cell incubated with the 12 nm-sized iron oxide nanoparticles seems to result from the susceptibility effect derived from the strong

magnetic moment of aggregates of the large-sized magnetic nanoparticles.[29]

In Vivo MR Imaging. For in vivo MR imaging, ESIONs (2.5 mg Fe/kg) were injected into a rat through its tail vein. After the injection of ESIONs, blood vessels were brightened on the T_1 weighted MR images, demonstrating that ESIONs can enhance T_1 relaxation in the circulating system (Figure 4). The bright signal of blood vessel can be maintained for 1 h on dynamic time-resolved MR angiography (Figure 4), showing that ESIONs can be used for T_1 enhanced blood pool MRI contrast agent. Blood pool imaging is important in clinical MR imaging because it can detect the myocardial infarction, renal failure, atherosclerotic plaque, thrombosis, and angiogenesis of tumor cells.[30] Long-term blood pool imaging is beneficial for steady-state imaging, which is critical to obtain high-resolution images.[31] For example, pulmonary artery imaging could clearly be obtained by the steady-state imaging using USPIOs.[32] ESIONs can be good T_1 contrast agent for steady-state imaging because they have a long blood half-life derived from their optimal particle size. The particles should not be so large to avoid uptake by the

Table 2. Relaxation Properties of the PO-PEG-Capped Iron Oxide Nanoparticles

size (nm)	r_1 (mM^{-1} s^{-1})	r_2 (mM^{-1} s^{-1})	r_2/r_1
2.2	4.78	17.5	3.67
3	4.77	29.2	6.12
12	2.37	58.8	24.8

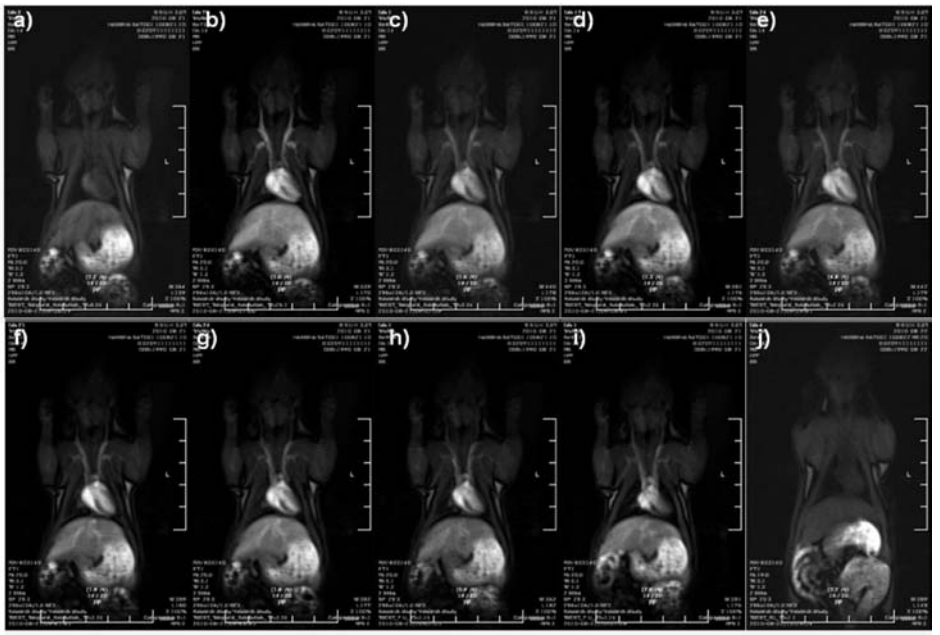

Figure 4. ESION-enhanced in vivo MR images with dynamic time-resolved MR sequence acquired at (a) 0 s and (b) 30 s, (c) 1 min, (d) 2 min, (e) 3 min, (f) 5 min, (g) 10 min, (h) 30 min, (i) 60 min, and (j) 1 day after the injection.

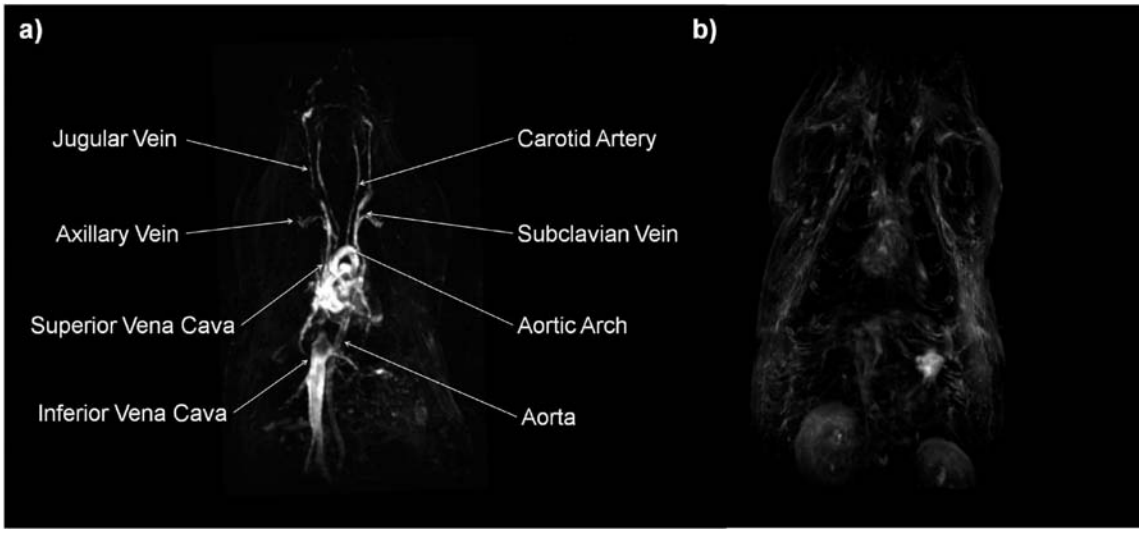

Figure 5. (a) ESION- and (b) DOTAREM-enhanced high-resolution blood pool MR images obtained using 3d-FLASH sequence.

reticuloendothelial system and should not be so small to keep the particles from being excreted through the kidney.[28] In contrast to ESIONs, gadolinium complex DOTAREM (Gd-DOTA), which is a commonly used T_1 MRI contrast agent, has a short blood half-life. Immediately after the injection of DOTAREM, in vivo MR image exhibited high contrast effect due to its high relaxivity, but the bright signal vanished rapidly (Figure S12 in the Supporting Information).

Long-term circulation can be evaluated by the time-dependent heart signal intensity. The ESION-enhanced MR signal intensity at heart was maintained at a high value for more than 1 h, while the DOTAREM-enhanced MR intensity dropped within 3 min (Figure S13a in the Supporting Information). The fast signal drop of gadolinium complexes can be explained by fast excretion through kidney, which can be confirmed by kidney signal intensity. The ESION-enhanced MR signal intensity of kidney was kept low during the entire data collection up to 60 min, while the DOTAREM-enhanced signal increased rapidly after the injection and remained high up to 10 min, which was 6 times stronger than that of ESIONs (Figure S13b in the Supporting Information). The fast clearance of DOTAREM was also confirmed by the MR signal in the kidney (Figure S14 in the Supporting Information).

The high-resolution blood pool MR image has been obtained using 3d-FLASH sequence, which has been frequently used to obtain high spatial resolution images. However, the long scan time (about 10 min) restricts the use of contrast agents, which have a short circulation time. The MR signal of the DOTAREM-enhanced blood pool MR image using 3d-FLASH sequence was weak because the gadolinium complex was rapidly excreted during the imaging (Figure 5b). In contrast, an excellent blood pool MR image was obtained using 3d-FLASH sequence after the injection of ESIONs. Various blood vessels including aorta, aortic arch, superior vena cava, inferior vena cava, axillary vein, jugular vein, carotid artery, and subclavian vein could be observed by ESION-enhanced imaging (Figure 5a, Supporting Information, movie 1). The resolution of the image was very high; even the 0.2 mm-sized vessels were able to be imaged. We could obtain the high-resolution blood pool T_1 enhanced MR image because of the long blood circulation time of ESIONs.

CONCLUSIONS

Uniform and extremely small-sized iron oxide nanoparticles (ESIONs) with diameters of <4 nm were synthesized by controlled thermal decomposition of iron−oleate complex in the presence of oleyl alcohol via heat-up process. The current synthetic procedure is very simple and can be easily scaled up to produce multigrams of the nanoparticles. The XRD pattern of ESIONs revealed maghemite crystal structure. Magnetization of ESIONs was much smaller than that of 12 nm-sized iron oxide nanoparticles because of their small magnetic moment and spin canting effect. ESIONs with a large number of surface Fe^{3+} ions with 5 unpaired electrons exhibited high r_1 relaxivities of > 4.7 mM^{-1} s^{-1} and low r_2/r_1 ratios of < 6.2, demonstrating that ESIONs can be used as efficient T_1 contrast agents. ESIONs with high r_1 relaxivity and long blood circulation time enabled high-resolution blood pool T_1-weighted MR imaging of various blood vessels with sizes down to 0.2 mm. The low toxicity, high r_1 relaxivity, long blood half-life, and low synthetic cost enable ESIONs to be competent T_1 MRI contrast agents for various clinical applications including diagnosis of the myocardial infarction, renal failure, atherosclerotic plaque, thrombosis, and angiogenesis of tumor cells.

ASSOCIATED CONTENT

Supporting Information. Detailed experimental procedures, XRD spectra and *d*-spacing value, FT-IR and TEM data for mechanism studies, field-dependent magnetization curves for 1.5, 2.2, 3, and 12 nm-sized iron oxide particles, DLS and TEM data of water-compatible ESIONs, cytotoxicity data of ESIONs including MTT, calcein-AM/PI, and 7-AAD assays, confocal microscopy image of RITC-labeled ESION-uptake cell, in vivo MR images enhanced by DOTAREM, signal intensity of heart and kidney, ESION- and DOTAREM-enhanced MR images of kidney, and complete ref 7b. This material is available free of charge via the Internet at http://pubs.acs.org.

AUTHOR INFORMATION

Corresponding Author

thyeon@snu.ac.kr; choiseunghong@gmail.com

Author Contributions

⊥These authors contributed equally.

ACKNOWLEDGMENT

T.H. acknowledges financial support by the Korean Ministry of Education, Science, and Technology through Strategic Research (2010-0029138) and World Class University (R31-10013) Programs of the National Research Foundation (NRF) of Korea. T.H and S.H.C. acknowledge financial support by Hanwha Chemicals Co.

REFERENCES

(1) (a) Na, H. B.; Hyeon, T. *J. Mater. Chem.* **2009**, *19*, 6267. (b) Brown, M. A.; Semelka, R. C. *MRI: Basic Principles and Applications*; Wiley-Liss: New York, 2003. (c) Na, H. B.; Song, I. C.; Hyeon, T. *Adv. Mater.* **2009**, *21*, 2133.

(2) (a) Bulte, J. W. M.; Kraitchman, D. L. *NMR Biomed.* **2004**, *17*, 484. (b) Wang, Y.-X. J.; Hussain, S. M.; Krestin, G. P. *Eur. Radiol.* **2001**, *11*, 2319. (c) Reimer, P.; Tombach, B. *Eur. Radiol.* **1998**, *8*, 1198. (d) Jun, Y.-w.; Huh, Y.-M.; Choi, J.-s.; Lee, J.-H.; Song, H.-T.; Kim, S.; Yoon, S.; Kim, K.-S.; Shin, J.-S.; Suh, J.-S.; Cheon, J. *J. Am. Chem. Soc.* **2005**, *127*, 5732. (e) Jun, Y.-w.; Seo, J.-W.; Cheon, J. *Acc. Chem. Res.* **2008**, *41*, 179. (f) Huh, Y.-M.; Jun, Y.-w.; Song, H.-T.; Kim, S.; Choi, J.-s.; Lee, J.-H.; Yoon, S.; Kim, K.-S.; Shin, J.-S.; Suh, J.-S.; Cheon, J. *J. Am. Chem. Soc.* **2005**, *127*, 12387. (g) Brooks, R. A. *Magn. Reson. Med.* **2002**, *47*, 388. (h) Weissleder, R.; Elizondo, G.; Wittenberg, J.; Rabito, C. A.; Bengele, H. H.; Josephson, L. *Radiology* **1990**, *175*, 489. (i) Weissleder, R.; Moore, A.; Mahmood, U.; Bhorade, R.; Benveniste, H.; Chiocca, E. A.; Basilion, J. P. *Nat. Med.* **2000**, *6*, 351. (j) Gao, J.; Liang, G.; Cheung, J. S.; Pan, Y.; Kuang, Y.; Zhao, F.; Zhang, B.; Zhang, X.; Wu, E. X.; Xu, B. *J. Am. Chem. Soc.* **2008**, *130*, 11828.

(3) Lee, N.; Kim, H.; Choi, S. H.; Park, M.; Kim, D.; Kim, H.-C.; Choi, Y.; Lin, S.; Kim, B. H.; Jung, H. S.; Kim, H.; Park, K. S.; Moon, W. K.; Hyeon, T. *Proc. Natl. Acad. Sci. U.S.A.* **2011**, *108*, 2662.

(4) Caravan, P. *Chem. Soc. Rev.* **2006**, *35*, 512.

(5) (a) Penfield, J. G.; Reilly, R. F. *Nat. Clin. Pract. Nephrol.* **2007**, *3*, 654. (b) Limbach, L. K.; Wick, P.; Manser, P.; Grass, R. N.; Bruinink, A.; Stark, W. J. *Environ. Sci. Technol.* **2007**, *41*, 4158.

(6) (a) Warsi, M. F.; Adams, R. W.; Duckett, S. B.; Chechik, V. *Chem. Commun.* **2010**, *46*, 451. (b) Endres, P. J.; Paunesku, T.; Vogt, S.; Meade, T. J.; Woloschak, G. E. *J. Am. Chem. Soc.* **2007**, *129*, 15760. (c) Taylor, K. M. L.; Kim, J. S.; Rieter, W. J.; An, H.; Lin, W.; Lin, W. *J. Am. Chem.*

Soc. **2008**, *130*, 2154. (d) Rieter, W. J.; Kim, J. S.; Taylor, K. M. L.; An, H.; Lin, W.; Tarrant, T.; Lin, W. *Angew. Chem., Int. Ed.* **2007**, *46*, 3680. (e) Kim, J. S.; Rieter, W. J.; Taylor, K. M. L.; An, H.; Lin, W.; Lin, W. *J. Am. Chem. Soc.* **2007**, *129*, 8962.

(7) (a) Hifumi, H.; Yamaoka, S.; Tanimoto, A.; Citterio, D.; Suzuki., K. *J. Am. Chem. Soc.* **2006**, *128*, 15090. (b) Park, Y. I.; et al. *Adv. Mater.* **2009**, *21*, 4467. (c) Bridot, J.-L.; Faure, A.-C.; Laurent, S.; Rivière, C.; Billotey, C.; Hiba, B.; Janier, M.; Josserand, V.; Coll, J.-L.; Elst, L. V.; Muller, R.; Roux, S.; Perriat, P.; Tillement, O. *J. Am. Chem. Soc.* **2007**, *129*, 5076.

(8) (a) Na, H. B.; Lee, J. H.; An, K.; Park, Y. I.; Park, M.; Lee, I. S.; Nam, D.-H.; Kim, S. T.; Kim, S.-H.; Kim, S.-W.; Lim, K.-H.; Kim, K.-S.; Kim, S.-O.; Hyeon, T. *Angew. Chem., Int. Ed.* **2007**, *46*, 5397. (b) Yu, T.; Moon, J.; Park, J.; Park, Y. I.; Na, H. B.; Kim, B. H.; Song, I. C.; Moon, W. K.; Hyeon, T. *Chem. Mater.* **2009**, *21*, 2272. (c) Choi, S.-H.; Na, H. B.; Park, Y. I.; An, K.; Kwon, S. G.; Jang, Y.; Park, M.; Moon, J.; Son, J. S.; Song, I. C.; Moon, W. K.; Hyeon, T. *J. Am. Chem. Soc.* **2008**, *130*, 15573. (d) An, K.; Kwon, S. G.; Park, M.; Na, H. B.; Baik, S.-I.; Yu, J. H.; Kim, D.; Son, J. S.; Kim, Y. W.; Song, I. C.; Moon, W. K.; Park, H. M.; Hyeon, T. *Nano Lett.* **2008**, *8*, 4252. (e) Gilad, A. A.; Walczak, P.; McMahon, M. T.; Na, H. B.; Lee, J. H.; An, K.; Hyeon, T.; van Zijl, P. C. M.; Bulte, J. W. M. *Magn. Reson. Med.* **2008**, *60*, 1. (f) Yang, H.; Zhuang, Y.; Hu, H.; Du, X.; Zhang, C.; Shi, X.; Wu, H.; Yang, S. *Adv. Funct. Mater.* **2010**, *20*, 1733. (g) Kim, T.; Momin, E.; Choi, J.; Yuan, K.; Zaidi, H.; Kim, J.; Park, M.; Lee, N.; McMahon, M. T.; Quinones-Hinojosa, A.; Bulte, J. W. M.; Hyeon, T.; Gilad, A. A. *J. Am. Chem. Soc.* **2011**, *133*, 2955.

(9) Roch, A.; Muller, R. N.; Gillis, P. *J. Chem. Phys.* **1999**, *110*, 5403.

(10) (a) Kodama, R. H. *J. Magn. Magn. Mater.* **1999**, *200*, 359. (b) Moser, A.; Takano, K.; Margulies, D. T.; Albrecht, M.; Sonobe, Y.; Ikeda, Y.; Sun, S.; Fullerton, E. E. *J. Phys. D: Appl. Phys.* **2002**, *35*, R157. (c) Jun, Y.-w.; Lee, J.-H.; Cheon, J. *Angew. Chem., Int. Ed.* **2008**, *47*, 5122.

(11) (a) Taboada, E.; Rodríguez, E.; Roig, A.; Oró, J.; Roch, A.; Muller, R. N. *Langmuir* **2007**, *23*, 4583. (b) Tromsdorf, U. I.; Bruns, O. T.; Salmen, S. C.; Beisiegel, U.; Weller, H. *Nano Lett.* **2009**, *9*, 4434. (c) Hu, F.; Jia, Q.; Li, Y.; Gao, M. *Nanotechnology* **2011**, *22*, 245604.

(12) Ouakssim, A.; Roch, A.; Pierart, C.; Muller, R. N. *J. Magn. Magn. Mater.* **2002**, *252*, 49.

(13) Park, J.; An, K.; Hwang, Y.; Park, J.-G.; Noh, H.-J.; Kim, J.-Y.; Park, J.-H.; Hwang, N.-M.; Hyeon, T. *Nat. Mater.* **2004**, *3*, 891.

(14) (a) Sun, S.; Zeng, H. *J. Am. Chem. Soc.* **2002**, *124*, 8204. (b) Sun, S.; Zeng, H.; Robinson, D. B.; Raoux, S.; Rice, P. M.; Wang, S. X.; Li, G. *J. Am. Chem. Soc.* **2004**, *126*, 273. (c) Peng, S.; Sun, S. *Angew. Chem., Int. Ed.* **2007**, *46*, 4155. (d) Hyeon, T.; Lee, S. S.; Park, J.; Chung, Y.; Na, H. B. *J. Am. Chem. Soc.* **2001**, *123*, 12798. (e) Hyeon, T. *Chem. Commun.* **2003**, 927. (f) Laurent, S.; Forge, D.; Port, M.; Roch, A.; Robic, C.; Elst, L. V.; Muller, R. N. *Chem. Rev.* **2008**, *108*, 2064. (g) Park, J.; Joo, J.; Kwon, S. G.; Jang, Y.; Hyeon, T. *Angew. Chem., Int. Ed.* **2007**, *46*, 4630. (h) Jana, N. R.; Chen, Y.; Peng, X. *Chem. Mater.* **2004**, *16*, 3931. (i) Yu, W. W.; Falkner, J. C.; Yavuz, C. T.; Colvin, V. L. *Chem. Commun.* **2004**, 2306. (j) Park, J.; Lee, E.; Hwang, N.-M.; Kang, M.; Kim, S. C.; Hwang, Y.; Park, J.-G.; Noh, H.-J.; Kim, J.-Y.; Park, J.-H.; Hyeon, T. *Angew. Chem., Int. Ed.* **2005**, *44*, 2872. (k) Jeong, U.; Teng, X.; Wang, Y.; Yang, H.; Xia, Y. *Adv. Mater.* **2007**, *19*, 33. (l) Kovalenko, M. V.; Bodnarchuk, M. I.; Lechner, R. T.; Hesser, G.; Schäffler, F.; Heiss, W. *J. Am. Chem. Soc.* **2007**, *129*, 6352. (m) Cheon, J.; Kang, N.-J.; Lee, S.-M.; Lee, J.-H.; Yoon, J.-H.; Oh, S. J. *J. Am. Chem. Soc.* **2004**, *126*, 1950. (n) Redl, F. X.; Black, C. T.; Papaefthymiou, G. C.; Sandstrom, R. L.; Yin, M.; Zeng, H.; Murray, C. B.; O'Brien, S. P. *J. Am. Chem. Soc.* **2004**, *126*, 14583. (o) Rockenberger, J.; Scher, E. C.; Alivisatos, A. P. *J. Am. Chem. Soc.* **1999**, *121*, 11595. (p) Kim, D.; Lee, N.; Park, M.; Kim, B. H.; An, K.; Hyeon, T. *J. Am. Chem. Soc.* **2009**, *131*, 454.

(15) (a) Teng, X.; Yang, H. *J. Mater. Chem.* **2004**, *14*, 774. (b) Lee, Y.; Lee, J.; Bae, C. J.; Park, J.-G.; Noh, H.-J.; Park, J.-H.; Hyeon, T. *Adv. Funct. Mater.* **2005**, *15*, 503.

(16) Na, H. B.; Lee, I. S.; Seo, H.; Park, Y. I.; Lee, J. H.; Kim, S.-W.; Hyeon, T. *Chem. Commun.* **2007**, 5167.

(17) Boyer, J.-C.; Manseau, M.-P.; Murray, J. I.; van Veggel, F. C. J. M. *Langmuir* **2010**, *26*, 1157.

(18) Cullity, B. D.; Stock, S. R. *Element of X-Ray Diffraction*, 3rd ed.; Prentice Hall: New York, 2001.

(19) (a) Adireddy, S.; Lin, C.; Palshin, V.; Dong, Y.; Cole, R.; Caruntu, G. *J. Phys. Chem. C* **2009**, *113*, 20800. (b) Teranishi, T.; Miyake, M. *Chem. Mater.* **1998**, *10*, 594. (c) Zeng, Y.; Hao, R.; Xing, B.; Hou, Y.; Xu, Z. *Chem. Commun.* **2010**, *46*, 3920. (d) Wang, D.; Li, Y. *J. Am. Chem. Soc.* **2010**, *132*, 6280.

(20) Kwon, S. G.; Piao, Y.; Park, J.; Angappane, S.; Jo, Y.; Hwang, N.-M.; Park, J.-G.; Hyeon, T. *J. Am. Chem. Soc.* **2007**, *129*, 12571.

(21) van Embden, J.; Mulvaney, P. *Langmuir* **2005**, *21*, 10226.

(22) (a) Chantrell, R. W.; Popplewell, J.; Charles, S. W. *IEEE Trans. Magn.* **1978**, *MAG-14*, 975. (b) Roca, A. G.; Marco, J. F.; Morales, M. P.; Serna, C. J. *J. Phys. Chem. C* **2007**, *111*, 18577. (c) Goya, G. F.; Berquó, T. S.; Fonseca, F. C.; Morales, M. P. *J. Appl. Phys.* **2003**, *94*, 3520.

(23) (a) Coey, J. M. D. *Phys. Rev. Lett.* **1971**, *27*, 1140. (b) Linderoth, S.; Hendriksen, P. V.; Bødker, F.; Wells, S.; Davies, K.; Charles, S. W.; Mørup, S. *J. Appl. Phys.* **1994**, *75*, 6583. (c) Yang, H.; Ogawa, T.; Hasegawa, D.; Takahashi, M. *J. Appl. Phys.* **2008**, *103*, 07D526.

(24) Müller, R.; Hergt, R.; Dutz, S.; Zeisberger, M.; Gawalek, W. *J. Phys.: Condens. Matter* **2006**, *18*, S2527.

(25) Jiles, D. *Introduction to Magnetism and Magnetic Materials*, 2nd ed.; Chapman & Hall: London, 1998.

(26) Pouliquen, D.; Le Jeune, J. J.; Perdrisot, R.; Ermias, A.; Jallet, P. *Magn. Reson. Imaging* **1991**, *9*, 275.

(27) Alkilany, A. M.; Nagaria, P. K.; Hexel, C. R.; Shaw, T. J.; Murphy, C. J.; Wyatt, M. D. *Small* **2009**, *5*, 701.

(28) Silver, J.; Ou, W. *Nano Lett.* **2005**, *5*, 1445.

(29) (a) Roch, A.; Gossuin, Y.; Muller, R. N.; Gillis, P. *J. Magn. Magn. Mater.* **2005**, *293*, 532. (b) Perez, J. M.; Joshephson, L.; O'Loughlin, T.; Högemann, D.; Weissleder, R. *Nat. Biotechnol.* **2002**, *20*, 816. (c) Matsumoto, Y.; Jasanoff, A. *Magn. Reson. Imaging* **2008**, *26*, 994.

(30) (a) Laissy, J. P.; Idée, J. M.; Loshkajian, A.; Benderbous, S.; Chillon, S.; Beaufils, H.; Schouman-Claeys, E. *J. Magn. Reson. Imaging* **2000**, *12*, 278. (b) Ruehm, S. G.; Corot, C.; Vogt, P.; Kolb, S.; Debatin, J. F. *Circulation* **2001**, *103*, 415. (c) Tombach, B.; Reimer, P.; Bremer, C.; Allkemper, T.; Engelhardt, M.; Mahler, M.; Ebert, W.; Heindel, W. *NMR Biomed.* **2004**, *17*, 500. (d) Allkemper, T.; Bremer, C.; Matuszewski, L.; Ebert, W.; Reimer, P. *Radiology* **2002**, *223*, 432. (e) Bremerich, J.; Bilecen, D.; Reimer, P. *Eur. Radiol.* **2007**, *17*, 3017. (f) Yancy, A. D.; Olzinski, A. R.; Hu, T. C-C.; Lenhard, S. C.; Aravindhan, K.; Gruver, S. M.; Jacobs, P. M.; Willette, R. N.; Jucker, B. M. *J. Magn. Reson. Imaging* **2005**, *21*, 432. (g) Weissleder, R; Lee, A. S.; Khaw, B. A.; Shen, T.; Brady, T. J. *Radiology* **1992**, *182*, 381. (h) Laissy, J. P.; Idee, J. M.; Loshkajian, A.; Benderbous, S.; Chillon, S.; Beaufils, H.; Schouman-Claeys, E. *J. Magn. Reson. Imaging* **2000**, *12*, 278. (i) Ruehm, S. G.; Corot, C.; Vogt, P.; Kolb, S.; Debatin, J. F. *Circulation* **2001**, *103*, 415.

(31) Bjørnerud, A.; Johansson, L. *NMR Biomed.* **2004**, *17*, 465.

(32) Ahlstrom, K. H.; Johansson, L. O.; Rodenburg, J. B.; Ragnarsson, A. S.; Akeson, P.; Borseth, A. *Radiology* **1999**, *211*, 865.